Coolant Flow Control Strategy to Reduce Chilled Water Temperature Fluctuations in an Adsorption Chiller

M. Hassan and Ahmed M. Bagabir[1]

Mechanical Engineering Department,
College of Engineering & Computer Sciences, Jazan University,
Jazan, Saudi Arabia

Abstract

Adsorption chillers, driven by low-grade waste heat, offer environmentally benign refrigeration with natural refrigerants like water, which has zero global warming potential, making them ideal for sustainable cooling in remote or off-grid settings. However, inherent chilled water temperature fluctuations during cyclic operation pose a major barrier to commercial viability, reducing system stability and user comfort. This study aims to mitigate these fluctuations while enhancing performance in a two-bed silica gel-water adsorption chiller. The key contribution is a novel control strategy integrating an expanded six-mode cycle (900 seconds) with PID-modulated cooling water flow approximated in discrete steps, n (3, 9, and 90), to follow the optimal profile. The numerical simulations were conducted using MATLAB. The outcome is validated by comparing the results against two established benchmarks: the conventional four-mode cycle and the ideal target cycle for adsorption chillers. The simulation results show significant reductions in evaporator temperature fluctuations to 0.9°C peak-to-peak for n=9, alongside coefficient of performance (COP) improvements up to 6% (to 0.476) and cooling capacity (CC) boosts up to 4.86% (to 14.62 kW) compared to conventional four-mode cycles. The n=9 configuration optimally balances stability and efficiency, with smoother refrigerant flow (0.04-0.10 kg/s), minimizing thermal imbalances. While the finest discretization (n=90) yields marginally higher performance of approximately 0.8% for COP and 0.4% for CC, the increase in temperature fluctuations creates a trade-off. These advancements enhance energy efficiency and reliability, positioning adsorption chillers as competitive alternatives for widespread sustainable applications in air conditioning and industrial cooling.

Keywords: Adsorption chiller, coolant flow control, chilled water temperature fluctuation, silica-gel/water, cycle time allocation

1. Introduction

Both absorption and adsorption refrigeration systems are thermally driven alternatives to conventional vapor compression systems [1-4]. Adsorption-based cooling cycles (ARCs) specifically use solid sorbents and can operate effectively with lower temperature heat sources [4-6]. Furthermore, adsorption systems are characterized by simpler, more robust designs with no moving parts, making them particularly well-suited for remote or off-grid applications [3, 5, 7, 8]. Moreover, ARCs have favorable environmental characteristics because they commonly use natural, non-toxic, and zero global warming potential refrigerants such as water paired with benign solid adsorbents like silica gel or zeolites, avoiding harmful synthetic refrigerants [9-11]. They can also utilize low-grade thermal energy sources such as solar or industrial waste heat, reducing electricity consumption and promoting low-carbon cooling

applications [3, 9, 12]. These characteristics position adsorption chillers as a green alternative for refrigeration, particularly in energy-efficient and eco-conscious applications [5].

ARCs generally exhibit a lower coefficient of performance (COP) compared to conventional vapor compression systems, due to inefficiencies in heat and mass transfer during the adsorption-desorption cycles [6, 8, 12-14]. Additionally, they require a larger adsorbent mass to achieve sufficient cooling capacity (CC), which increases the system size and material costs, limiting compactness and practical applications [3, 7, 8, 10, 12, 13]. This can increase material and energy requirements unless optimized through improved adsorbents or heat-recovery techniques [5, 13]. Adsorption chillers typically achieve a coefficient of performance (COP) ranging from 0.3 to 0.7 under standard conditions, with performance enhanced in combined systems or through composite adsorbents that improve heat and mass transfer rates [2, 9, 12]. Optimum operating conditions include desorption temperatures of 60-90°C, and adsorption temperatures below 35°C, which maximize CC and COP when utilizing low-grade heat sources [3, 5, 14-16].

Adsorption chillers provide sustainable refrigeration by utilizing low-grade waste heat and natural refrigerants, but their performance is limited by inefficiencies in cycle configurations [3-8]. Modified adsorption refrigeration cycle (ARC) configurations, including heat and mass recovery cycles, pre-heating/pre-cooling phases, multi-bed or multi-stage arrangements, and combined absorption-adsorption systems, enhance cooling capacity and COP by reducing sensible heat losses, dead times, and enabling continuous operation with better regeneration at lower temperatures [1, 2, 5, 9, 11, 13, 14, 17-21]. The six-mode cycle in two-bed silica gel-water adsorption chillers generally outperforms the conventional four-mode cycle, offering higher cooling capacity, improved COP, and reduced temperature fluctuations when cycle times are optimally allocated, though gains depend on system configuration and operating conditions [22, 23]. Optimal cycle times for silica gel-water adsorption systems typically range from 600 to 1600 seconds, depending on system design and operating conditions [22-25]. Cycle time optimization is critical [3, 9, 12, 14, 16, 22, 23, 26-29]. The shorter cycles increase specific cooling capacity but reduce COP due to incomplete processes, while the longer cycles improve COP and stability. Moreover, longer pre-heating/pre-cooling (switching) times reduce effective cycle duration, lowering COP and cooling power due to increased sensible heat losses, while minimizing these times through heat recovery or design improvements extends productive adsorption/desorption phases for greater efficiency [9, 12, 14, 16, 22, 30].

Chilled-water temperature fluctuations of 2-5 °C represent a major drawback in adsorption chillers, stemming from intermittent adsorption/desorption, bed switching phases, and transient heat/mass transfer, leading to unstable cooling output, reduced effective COP, and lower user comfort [2, 5, 9, 12, 14, 16, 26, 27, 31]. These fluctuations can be reduced through multi-bed configurations, advanced cycle designs, improved evaporator/nozzle heat transfer, and optimized adsorption/desorption timing, yielding up to 15.6% higher cooling capacity [1, 20, 22, 23, 26, 31, 32]. Adjusting chilled water flow rate stabilizes evaporator outlet temperature (e.g., 7-8 °C), with higher rates enhancing heat transfer for reduced swings and improved performance, while lower rates may exacerbate fluctuations [1, 33-39].

A significant challenge, identified through the literature review, is the lack of universal optimal parameters for flow rate and timing, as only system-specific results have been reported thus far. This research addresses limitations by developing and evaluating a new control strategy for the cooling water flow within the adsorbent bed of a two-bed adsorption chiller. The primary objective is to reduce fluctuations in the delivered chilled water temperature during cyclic steady-state operation, thereby overcoming a major drawback of conventional adsorption cooling devices. The study uses a 900-second

cycle time and a six-mode operational scheme, unlike the traditional four-mode cycle. The new timing and mode allocation are integrated with precise modulation of the cooling water flow rate via PID control, using 3, 9, and 90 discrete steps to approximate the optimal flow profile. The research analyzes and validates the performance of the proposed advanced scheme by comparing its key metrics to those of the conventional two-bed silica gel-water cycle and the ideal constant evaporator temperature cycle. This work strongly aligns with sustainable engineering goals by advancing a low-carbon, waste-heat-driven cooling technology. The successful stabilization of the chilled water temperature and the simultaneous performance boost provide a clear pathway to commercial viability. The results will directly guide practical design and optimization for off-grid and low-grade waste-heat-driven adsorption chiller applications.

The next section, system description of the two-bed adsorption chiller, details the system configuration and six-mode cycle time. This is followed by methodology section, which presents the governing equations for adsorption isotherms and rate, mass balance, energy balances, flow control strategy, PID control and discrete multi-step flow rate modulation, and simulation procedure. The fourth section, results and discussion, presents simulation results and analysis, including performance characteristics, improved COP, and reduced temperature fluctuation. Finally, the conclusions section effectively summarizes the research's key findings, synthesizing the insights derived from the study. It also incorporates implications, limitations, and recommendations for future work.

2. System Description

Figure 1 shows the schematic diagram of a two-bed silica gel-water adsorption cooling cycle. This cycle includes an evaporator, a condenser, and two sorption beds. Each bed alternates between the adsorption phase (producing cooling) and the desorption phase (regenerating the adsorbent using heat input). Valves V1–V4 regulate which bed is active at any given time. During the adsorption-evaporation process, which occurs at evaporator pressure ($Pevap$), the refrigerant (water) evaporates at the evaporation temperature ($Tevap$) and absorbs heat ($Qevap$) from the chilled water. The resulting vapor is adsorbed by the silica gel in bed 1, where cooling water removes the heat of adsorption ($Qads$). In the parallel desorption-condensation process at condenser pressure ($Pcond$), bed 2 (the desorber) is heated to the desorption temperature ($Tdes$) by the driving heat source ($Qdes$). The desorbed water vapor then flows to the condenser, where it is cooled to the condensation temperature ($Tcond$) by cooling water, which extracts the heat of condensation ($Qcond$). Once the pressures in the desorber and adsorber approach those of the condenser and evaporator, respectively, the valves between bed 2 and the evaporator, as well as between bed 1 and the condenser, are opened to facilitate refrigerant flow from the evaporator to the adsorber bed and from the desorber to the condenser.

Figure 2 presents a Clapeyron (P-T-W) diagram for an adsorption chiller, plotting pressure (Pa) on a logarithmic scale against temperature (°C). The diagram is overlaid with diagonal lines representing constant refrigerant uptake (isosteric), ranging from 0.01 to 0.15 kg/kg of silica gel. Two thermodynamic cycles are represented on this grid (Fig. 2) to compare performance: the conventional cycle and the constant evaporator temperature cycle, which serves as the ideal benchmark (or target) for evaluating controlled strategies like PID flow modulation. Both cycles trace the four phases of the adsorption process: isosteric heating, isobaric desorption, isosteric cooling, and isobaric adsorption. The most significant deviation between the two cycles occurs during the adsorption phase (the bottom segment of the loop). The conventional cycle shows a distinct dip in pressure as the process moves leftward, indicating that the evaporator pressure (and consequently temperature) drops significantly during operation, which reduces the driving force for mass transfer (Fig. 2). In contrast, the target cycle

maintains a perfectly flat, horizontal path during this phase. This isobaric behavior confirms that the flow-modulation control can successfully stabilize the evaporator pressure. By eliminating the pressure drop observed in the conventional cycle, the controlled strategy sustains more favorable adsorption conditions, which directly enhances the COP and CC [33-36].

The conventional two-bed adsorption cycle is completed using four distinct operational modes (as detailed in Table 1). These four modes are symmetrically split into two pairs of equal duration. Two modes (A and C) are designated for active adsorption or desorption processes, while two additional modes (B and D) are used for pre-heating or pre-cooling the beds (Table 1). The best cycle time for silica gel-water adsorption chillers depends on operating conditions. The proposed cooling-water flow control strategy for the adsorber involves six distinct operational modes, which are fully detailed in Table 2. These modes dictate the cycle timing for the two-bed silica gel-water adsorption chiller, operating with a total cycle time of 900 seconds. Notably, 900 seconds is often found to be the closest to the optimal cycle time for maximizing both cooling capacity and efficiency under typical operating conditions [23-25]. The modes are labeled A, B, C, D, E, and F, with respective durations of 30, 360, 60, 30, 360, and 60 seconds, respectively (Table 2). The unequal distribution ensures that the sorption element has an ample duration to efficiently lower its temperature from the high desorption level down to the required adsorption level before the main cooling production phase begins [9, 12, 14, 16, 22, 30]. Specifically, the pre-cooling phases last for 60 seconds, which is twice the duration of the 30-second pre-heating phases. This strategy is implemented to enhance adsorption performance, given that adsorption kinetics in RD silica gel-water systems are inherently slower than their desorption kinetics. The unequal allocation of time for heat recovery is noteworthy. The pre-cooling phases last for 60 seconds, which is twice as long as the 30-second duration of the pre-heating phases. This approach is intended to improve adsorption performance, as the adsorption kinetics in silica gel-water systems are slower than the desorption kinetics [40, 41].

3. Methodology

The framework is built around the governing equations for adsorption isotherms, adsorption rate, and the fundamental mass and energy balances for all major components (adsorber, desorber, condenser, and evaporator). It also details the equations for the key performance metrics. This section will detail the design of the PID controller and the process for discretizing the cooling water flow strategy, as well as the convergence criteria for the simulation. The computational efficiency and standard nature of the simulation are maintained through common assumptions, such as neglecting the gas-phase refrigerant volume and using lumped-parameter models.

3.1 Adsorption Isotherms

In this study, the modified Freundlich model, known as the Saha-Boelman-Kashiwagi (SBK) equation, is used to evaluate the adsorption isotherms of the RD silica gel-water pair. The equation can be written as [42]:

$$W = A(T_s)\left[\frac{P_s(T_w)}{P_s(T_s)}\right]^{B(T_s)} \tag{1}$$

Where W denotes the adsorption uptake (kg/kg of silica gel) at equilibrium conditions. $P_s(T_w)$ represents the saturation vapor pressure at the water vapor temperature, T_w, while $P_s(T_s)$ corresponds to the saturation vapor pressure at the adsorbent (silica gel) temperature, T_s. The adjustable parameter $A(T_s)$ and $B(T_s)$ are defined as [42]:

$$A(T_s) = A_0 + A_1 T_s + A_2 T_s^2 + A_3 T_s^3 \tag{2}$$

$$B(T_s) = B_0 + B_1 T_s + B_2 T_s^2 + B_3 T_s^3 \tag{3}$$

The numerical values of coefficients A_0 - A_3 and B_0 - B_3 were determined via a least-squares fit to the experimental data for the silica gel-water pair and are listed in Table 3 [42].

3.2 Adsorption Rate

As the adsorption process in the adsorbent bed is considered to be controlled by macroscopic diffusion into the particle bed, the adsorption rate can be expressed linearly as [43, 44]:

$$\frac{dw}{dt} = \frac{15 D_s}{R_p^2}(W - w) \tag{4}$$

Where $15D_s/R_p^2$ denotes the overall mass transfer coefficient. Here, R_p is the adsorbent particle radius. The surface diffusivity in the adsorption rate model, D_s, can be expressed as:

$$D_s = D_{so} \exp\left(\frac{E_a}{RT}\right) \tag{5}$$

In this equation, R is the universal gas constant (8.314 J/mol·K) and T is adsorbent temperature. The required numerical parameters for the silica gel-water system are defined as follows: the pre-exponential term (D_{so}) is 2.54×10^{-4} m^2/s, and the activation energy for surface diffusion (Ea) is 42 kJ/mol, respectively [43, 44].

The mass balance of refrigerant is written by neglecting the gas phase as:

$$\frac{dM_w}{dt} + M_s\left(\frac{dw_{ads}}{dt} + \frac{dw_{des}}{dt}\right) = 0 \tag{6}$$

Where M_w is the mass of the water in the liquid phase, and M_s is the mass of the adsorbent (silica gel) packed in each of the two identical adsorbent beds. The subscripts *ads* and *des* denote the adsorption and desorption processes, respectively.

3.3 Energy Balance

To simplify the energy and heat balance equations for the adsorption system, a lumped model approach is used (45, 33). This approach assumes that the adsorbent, adsorbate, and heat exchanger metal are all at the same uniform temperature at any given time. Additionally, the mass of refrigerant vapor and heat losses to the ambient are considered negligible. Under these assumptions, the adsorber and desorber energy balances can be described by [33, 45]:

$$\left[(Mc_p)_{bed} + M_s q_i c_p\right]\frac{dT_{i,bed}}{dt} = \alpha M_s\left(\frac{dq_i}{dt}\right)q_{st} + (\dot{m}c_p)_{w,bed}\left(\beta T_{Hw} + (1-\beta)T_{Cw} - T_{Ow,bed}\right) \tag{7}$$

The coefficients α and β are operational switches, α is set to 0 during the switching time and 1 during the active adsorption or desorption phases, while β is 0 during pre-cooling and adsorption, and 1 during pre-heating and desorption. The bed is identified by the subscript i. The terms in Eq. (7) represent the energy balance of the bed system (metal, adsorbent, and adsorbed refrigerant). The term on the left-hand side of Eq. (7) represents the change in internal energy of the bed. The first term on the right-hand side of Eq. (7) accounts for the heat involved in adsorption or desorption. The second term reflects the total heat exchanged with the cooling or hot water, along with the heat required to superheat the incoming refrigerant vapor from the evaporator.

The outlet water temperature from the adsorbent bed can be expressed as [33, 45]:

$$T_{Ow,bed} = T_{i,bed} + \left(\left(\beta T_{Hw} + (1-\beta)T_{Cw}\right) - T_{i,bed}\right)\exp\left[\frac{(UA)_{bed}}{(\dot{m}c_p)_{w,bed}}\right] \tag{8}$$

The following equation can be used for the energy balance in the condenser [33, 45]:

$$(Mc_p)_{cond}\frac{dT_{cond}}{dt} = \alpha M_s\left(\frac{dw_{des}}{dt}\right)h_{fg} + \alpha(\dot{m}c_p)_{w,cond}\left(T_{Cw} - T_{Ow,cond}\right) + c_{p-phase}T_{cond}M_s\frac{dw_{ads}}{dt} \tag{9}$$

The term on the left-hand side describes the sensible heat required for the condenser metal mass. The right-hand side of the equation consists of three terms: the heat generated by the desorbed refrigerant, the total heat released to the cooling fluid, and the heat removed by the liquid condensate as it exits the evaporator.

The outlet water temperature from the condenser can be expressed by [33, 45]:

$$T_{Ow,cond} = T_{cond} + \left(T_{w,in} - T_{cond}\right)\exp\left[\frac{(-UA)_{cond}}{(\dot{m}c_p)_{w,cond}}\right] \tag{10}$$

The evaporator energy balance equation is given by [33, 45]:

$$(Mc_p)_{evap}\frac{dT_{evap}}{dt} = -M_s\left(\frac{dw_{ads}}{dt}\right)h_{fg} + (\dot{m}c_p)_{chill}\left(T_{chill,in} - T_{chill,o}\right) + c_{p-phase}T_{cond}M_s\frac{dw_{ads}}{dt} \tag{11}$$

The left-hand side term describes the sensible heat required by both the liquid refrigerant and the metal mass within the evaporator. The right-hand side of the equation indicates three distinct terms: the heat necessary for the evaporation of the adsorbed refrigerant, the total heat supplied by the chilling water, and the sensible heat used to cool the incoming condensate. The chilled water outlet temperature, $T_{chill,o}$, is given by [33, 45]:

$$T_{chill,o} = T_{evap} + \left(T_{chill,in} - T_{evap}\right)\exp\left[\frac{(-UA)_{evap}}{(\dot{m}c_p)_{chill}}\right] \tag{12}$$

During cyclic steady-state operation, the evaporator temperature remains constant. This means that the term on the left side of Eq. (11), which represents the rate of sensible heat change (dT_{evap}/dt), is zero. Consequently, rearranging Eq. (11) yields the following [33, 45]:

$$\left.\frac{dw_{ads}}{dt}\right|_{T_{evap}=const} = \frac{(\dot{m}c_p)_{chill}\left(T_{chill,in} - T_{chill,o}\right)}{M_s(h_g - C_{p-phase}T_{cond})} \tag{13}$$

3.4 System Performance

The performance of the two-stage adsorption cycle is primarily evaluated by calculating three key metrics: cooling capacity, specific cooling capacity, and the coefficient of performance [33, 45].

$$\text{Cooling capacity (CC)} = \frac{(\dot{m}C_p)_{chill}\int_0^{t_{cycle}}(T_{chill,in} - T_{chill,o})dt}{t_{cycle}} \tag{14}$$

For the constant delivered chilled water temperature, the CC does not vary with time and can be expressed as:

$$Q_{chill}^{cycle} = \left(\dot{m}C_p\right)_{chill}\left(T_{chill,in} - T_{chill,o}\right) \quad (15)$$

The specific cooling capacity (SCC), which is the cooling capacity per kilogram of silica gel, can be expressed as

$$SCC = \frac{Q_{chill}^{cycle}}{W_s} \quad (16)$$

The coefficient of performance (COP) can be described as:

$$COP = \frac{\left(\dot{m}C_p\right)_{chill}\left(T_{chill,in} - T_{chill,o}\right)t_{cycle}}{\int_0^{t_{cycle}} \left(\dot{m}C_p\right)_{w,bed}\left(T_{Hw} - T_{Ow,bed}\right)dt} \quad (17)$$

3.5 Flow Control Strategy

The proposed cycle utilizes six distinct operational modes per sorption element (Table 2), representing an expansion from the four modes employed in the conventional system (Table 1). The specific control strategy for the cooling water flow rate is implemented through the following three-step procedure:

1. Calculate the required adsorption rate: Determine the adsorption rate necessary to maintain a constant evaporator temperature using Eq. (11). The equation assumes a constant chilled water temperature throughout the cycle $\left(dT_{evap}/dt = 0\right)$.
2. Estimate bed temperature: Use an iterative method to estimate the bed temperature that makes the left-hand side of Eq. (4) equal to the left-hand side of Eq. (13):

$$dw_{ads}/dt = (dw_{ads}/dt)_{T_{evap=const}}$$

3. Determine cooling water flow rate: Substitute the bed temperature calculated in step 2 into equations (7) and (8) to determine the necessary cooling water flow rate. This calculated flow rate will ensure that the evaporator temperature remains consistent.

3.6 PID Control and Discrete Multi-Step Flow Rate Modulation

The proposed control strategy integrates a proportional-integral-derivative (PID) controller with a discrete *n*-step approximation to dynamically modulate the cooling water flow rate $\dot{m}_{Cw}$ in the adsorber bed. This method aims to maintain a constant evaporator temperature ($Tevap$) at the target set point of $T_{evap,const} = 8.7^{o}C$, which stabilizes the chilled water outlet temperature ($Tchill,o$) and reduces fluctuations during the adsorption phase. The PID controller is implemented as an external feedback mechanism in the simulation using MATLAB, mimicking a real-world setup. It adjusts a variable-speed pump or proportional valve that controls the flow of cooling water to the adsorber. Unlike fixed-flow strategies used in conventional cycles, this active control system responds dynamically to changes in the system.

The PID controller operates as a closed-loop system, monitoring $Tevap$, with the error defined as $e(t) = T_{evap,const} - T_{evap,actual}$. This indirectly stabilizes $Tchill,o$, which is calculated from the evaporator energy balance (Eq. 12) and is closely tied to $Tevap$ under steady-state assumptions. The cooling water mass flow rate to the adsorber $\dot{m}_{Cw}$, which is adjusted to minimize the error $e(t)$. The standard equation for the PID output $u(t)$ is:

$$u(t) = K_p e(t) + K_i \int_0^t e(t)\,dt + K_d \frac{de(t)}{dt} \quad (18)$$

Where K_p, K_i, and K_d are the proportional, integral, and derivative gains, respectively.

To approximate the continuous PID signal, the strategy discretizes the flow rate into n uniform levels (n=3, 9, or 90), ranging from a minimum flow rate ($\dot{m}_{Cw,min}$) at the start of adsorption (when heat release is high) to a maximum ($\dot{m}_{Cw,max}$) at the end (when heat release diminishes). This choice of n values spans coarse (n=3) for simplicity, intermediate (n=9) for optimal balance, and fine (n=90) for near-continuous approximation to enable systematic evaluation of stability, efficiency, and practicality against the ideal flow profile. The discretization converts the continuous PID output to the nearest discrete step as follows:

- The PID computes a continuous target flow rate based on the error $e(t)$.
- This target is rounded to the nearest discrete level defined by an arithmetic progression of flow increments.

The required cooling water flow rate for discrete steps n during the half-cycle time can be calculated using:

$$\dot{m}_{Cw}(n) = \dot{m}_{Cw\ \min} + (n-1)\Delta\dot{m}_{Cw} \quad (19)$$

The incremental increase in the cooling water flow rate ($\Delta\dot{m}_{Cw}$) for each step is given by:

$$\Delta\dot{m}_{Cw} = \frac{\dot{m}_{Cw\max} - \dot{m}_{Cw\min}}{n-1} \quad (20)$$

The terms $\dot{m}_{Cw\min}$ and $\dot{m}_{Cw\max}$ are predetermined boundaries based on the ideal flow profile. The PID does not directly control the duration of each step, instead, it sets a target flow that is snapped to the nearest discrete level, $\dot{m}_{Cw}(n)$, at each simulation time step.

3.7 Simulation Procedure

The simultaneous solutions of the mathematical models, which were described above, were carried out using the MATLAB computer package. This approach allowed for the efficient handling of the transient, coupled heat and mass transfer processes in the two-bed silica gel-water adsorption chiller. Custom scripts incorporated operational switches (α and β) to toggle between adsorption/desorption phases and pre-heating/pre-cooling modes over a typical 900-second cycle. Throughout this process, the parameters of all ordinary differential equations (Eqs. 1 to 16) were dynamically updated according to the specific operation mode. A tight solution tolerance 1×10^{-6} was applied to all parameters. The program continued to simulate the cyclic operation until it reached the cyclic steady-state condition. This convergence was successfully confirmed when two criteria were met simultaneously:

1. The absolute difference between the instantaneous coefficient of performance (COP) and the COP of the previous time step did not exceed 5×10^{-4}.
2. The temperature of each bed changed by less than 0.01°C compared to its value at the previous cycle time.

4. Results and Discussion

Figure 3 presents the variation of cooling-water mass flow rate (kg/s) over a complete adsorption/desorption cycle lasting 900 seconds. It compares the ideal flow profiles required to maintain constant evaporator temperatures of 8.7 °C, with the actual flow delivered by a PID controller implemented in discrete steps. The ideal curve is smooth and S-shaped, while the PID-controlled (3-step

and 9-step) flows appear as staircase patterns. To achieve a perfectly constant chilled-water outlet temperature, cooling-water flow must vary significantly and continuously throughout the cycle. The finer 9-step (n=9) PID control closely tracks the ideal profile, whereas the coarse 3-step (n=3) version shows noticeable deviations (Fig. 3). Both discrete-step implementations demonstrate that simple multi-stage valve control can effectively approximate the continuous flow variation needed to stabilize evaporator temperature. At the start of the adsorption phase, the adsorption rate is high, so only a very low cooling-water flow rate is needed to remove the released heat of adsorption. Toward the end of the adsorption phase, the adsorption rate decreases significantly, generating much less heat. Consequently, the cooling water flow rate must be significantly increased to maintain the desired evaporator temperature, as shown in Fig. 3.

Figure 4 presents the evaporator (chilled-water outlet) temperature profile over one complete adsorption/desorption cycle for three operating strategies using cooling-water flow-rate control, compared with the conventional fixed-flow cycle. The ideal constant-temperature cycle keeps the evaporator temperature constant at the target of 8.7 °C, represented as a horizontal line in Fig. 4. In the conventional cycle, the temperature fluctuates strongly between approximately 8 °C and 11.7 °C, with large peaks and valleys synchronized with bed switching. The coarse PID control with 3 steps (n=3) substantially reduces these swings but still exhibits ripples of about ±1 °C around the target. The 9-step control (n=9) performs significantly better, staying much closer to 8.7 °C with only minor deviations, as shown in Fig. 4. The finest 90-step control (n=90) almost perfectly follows the ideal constant-temperature profile. This demonstrates that very fine or near-continuous flow-rate adjustment can virtually eliminate temperature fluctuations and deliver highly stable chilled-water output.

The coefficient of performance (COP) of an adsorption chiller as a function of the adsorber (hot-water) temperature, ranging from 65 °C to 85 °C, is illustrated in Fig. 5. The graph compares five different operating methods, which include the theoretical target cycle, the conventional cycle, and three strategies that employ PID control for flow modulation, specifically using 3, 9, and 90 discrete steps. All COP values range between approximately 0.38 and 0.48, illustrating the efficiencies achievable at these specific hot-water temperatures. The target cycle consistently yields the highest COP across the entire temperature range, showing a steep initial increase in performance at lower temperatures (Fig. 5). In stark contrast, the conventional cycle delivers the lowest COP, remaining nearly flat and significantly below the ideal maximum. The integration of a six-mode cycle with discrete-step PID flow control demonstrates a marked improvement over the conventional fixed-flow system. The efficiency gain is directly linked to the precision of the modulation. The 90-step control strategy compensates for most of the performance loss, resulting in a performance curve that nearly matches the target cycle above 80 °C (Fig. 5). This evidence confirms that employing finer (near-continuous) modulation of the cooling water flow effectively brings the chiller's operating performance very close to its theoretical maximum.

Figure 6 illustrates the relationship between the cooling capacity, CC and the adsorber temperature for an adsorption chiller. Five operational strategies are presented for comparison. These include the target cycle, the conventional cycle, and three PID control strategies for modulating the cooling-water flow in discrete steps: a coarse 3-step strategy, a 9-step strategy, and a very fine 90-step strategy. The graph illustrates that capacity consistently increases as the adsorber temperature rises throughout all cycles. The target cycle establishes the upper performance limit, showing a linear increase in CC from approximately 7.7 kW at 65 °C to nearly 15 kW at 85 °C. The conventional cycle consistently produces the lowest capacity, falling about 1-2 kW short of the ideal benchmark across the measured temperature range (Fig. 6). All PID-controlled strategies achieve a significant improvement in capacity relative to the conventional cycle. The effectiveness of the control is directly proportional to the number of steps

utilized: the 3-step (n=3) version provides a noticeable performance gain, the 9-step (n=9) version operates much closer to the ideal curve, and the 90-step (n=90) control essentially recovers almost all lost capacity, becoming virtually superimposed on the target cycle curve. This observation confirms that fine, near-continuous flow modulation is a highly effective method for maximizing the operational CC of these chillers, bringing performance close to the theoretical maximum (Fig. 6).

Table 4 compares the PID-controlled discrete-step schemes with the conventional adsorption cycle using two criteria: chilled-water temperature stability (peak-to-peak and standard deviation, SD) and maximum performance (coefficient of performance, COP, and cooling capacity, CC). The 9-step PID control (n=9) strategy exhibits the lowest peak-to-peak fluctuation of 0.9°C among the controlled cycles, signifying the most stable chilled-water temperature output. The results underscore the advantages of PID control strategies in enhancing both temperature stability and overall system performance. The conventional cycle exhibits the highest standard deviation (1.34°C), indicating its significant temperature instability, with a baseline COP of 0.451 and a CC of 13.94 kW (Table 4). In contrast, the 9-step PID control strategy attains the lowest standard deviation (0.30°C), ensuring the most consistent chilled-water outlet temperature near the target value throughout the cycle. It also improves COP to 0.476 (a 5.6% gain) and CC to 14.62 kW (a 4.9% increase) over the conventional baseline (Table 4). Further refinement with PID (n=90) yields even higher performance, with a COP of 0.478 (6.0% improvement) and CC of 14.74 kW (5.7% boost). It exhibits slightly higher fluctuation (1.2°C peak-to-peak) than 9-step strategy, suggesting a trade-off where finer steps increase efficiency but may not always minimize swings as effectively as intermediate discretization (Table 4).

For practical applications in adsorption chillers, 9 steps are usually sufficient instead of 90 steps. The marginal improvements in COP (from 0.476 to 0.478, or ~0.4% relative gain) and CC (from 14.62 kW to 14.74 kW, or ~0.8% relative gain) do not justify the added complexity of finer control steps, especially since n=90 results in higher peak-to-peak fluctuations (1.2 °C vs. 0.9 °C). The 9-step strategy already achieves excellent temperature stability (lowest SD 0.30°C) and substantial performance uplift over the conventional baseline. This prioritizes user comfort and system reliability without requiring near-continuous modulation that could demand more sophisticated valves, sensors, or computational resources. If maximum efficiency is crucial in high-demand commercial settings, and minor fluctuations are acceptable, using 90 step may be beneficial, otherwise, 9 steps provides the best balance of stability and performance improvements. The discrepancy where near-continuous modulation (n=90) yields higher evaporator temperature swings (1.2°C peak-to-peak) than 9 steps (0.9°C) can be justified as follows. In the PID controller, the output $u(t)$ is adjusted based on the instantaneous error $e(t)$ and then discretized into n steps for the cooling water flow rate (Eqs. 18-20). In this highly transient, lumped-parameter adsorption model, fine discretization (n=90) enables highly accurate and frequent flow adjustments [46]. However, small unavoidable numerical noise, simulation artifacts, or minor phase lags in heat/mass transfer equations (e.g., Eqs. 4-7) can amplify these rapid changes, translating into slight oscillations [46]. Conversely, the coarser n=9 scheme offers a "buffer" with fewer, more robust steps, inherently damping high-frequency fluctuations. This leads to a smoother overall temperature profile, even though the flow appears as a coarser staircase approximation (as illustrated in Fig. 3) compared to the nearly continuous profile for the case with n=90. Adjusting the PID gains, such as lowering (K_d) (see Eq. 18), for high values of n could help alleviate this issue. However, this situation emphasizes the sensitivity of control in such nonlinear systems [46].

Figure 7 shows the instantaneous refrigerant mass flow rate, ranging from approximately 0.04 to 0.10 kg/s, within two adsorbent beds over a complete 900-second cycle. The graph compares two distinct operating modes, the conventional cycle and a controlled 9-step strategy. The cycle demonstrates the alternating nature of the system, as the mass in Bed 1 increases (adsorption), the mass in Bed 2 decreases (desorption/regeneration), and vice versa. A distinct difference in the rate of mass change is visible between the two strategies. In the conventional cycle, the curves exhibit steep slopes at the beginning of each phase, indicating that refrigerant is adsorbed or desorbed very rapidly initially, but the rate decays significantly as the phase progresses (Fig. 7). This curvature implies a pulsating flow rate that is uneven over time. Conversely, the 9-step strategy (n=9) produces much more linear mass profiles (Fig. 7). The refrigerant uptake and release occur at a nearly constant rate, creating "mirror image" behavior between the two beds. This linearity in mass change indicates a smooth, continuous flow of refrigerant, which validates the claim that flow modulation stabilizes the process, reducing fluctuations and improving the average cooling capacity (CC) compared to the conventional fixed-flow approach.

The present proposed six-mode cycle with discrete multi-step PID flow control for the adsorber cooling water surpasses prior methods (e.g., multi-bed configurations, cycle time optimization, and chilled water flow adjustments) in several key ways:

- Superior temperature stability: Prior methods typically reduce chilled water fluctuations to 2-5°C (e.g., via multi-bed setups [20], or flow rate adjustments [33, 34]). The proposed approach achieves 0.9°C peak-to-peak (standard deviation 0.30°C) for n=9 steps, nearing ideal constant output (8.7°C target) without multi-bed complexity. This improves user comfort and integration in specialized applications, such as air conditioning.
- Enhanced efficiency and capacity: It improves COP by up to 6% (to 0.478) and CC by 5.7% (to 14.74 kW) over conventional four-mode baselines, outperforming the gains of prior methods (e.g., up to 15.6% CC increase in multi-bed systems [1], but with higher fluctuations). Smoother refrigerant flow (0.05–0.10 kg/s, linear mass profiles) minimizes thermal imbalances, unlike the pulsating flows in conventional or less integrated priors.
- Practicality and integration: Unlike system-specific optimizations in priors (e.g. absorption analysis [35] or improved two-bed design [36]), the asymmetric six-mode (doubled pre-cooling time) combined with discrete PID (n=9 optimal) provides a universal, balanced strategy. It simplifies the complexity of continuous modulation (e.g., n=90's marginal gains but higher fluctuations) while addressing the lack of unified flow-timing parameters in previous models, making it more feasible for sustainable, waste-heat-driven cooling.

5. Conclusion

Adsorption cooling is vital for sustainable technology, however, its widespread use is greatly hindered by a significant technological challenge: considerable temperature fluctuations in the chilled water produced. This thermal instability undermines user comfort and limits its applicability in precise industrial and commercial settings. This research focused on addressing the fundamental instability issue in two-bed adsorption chillers. The main objective was twofold. First, to develop and simulate a new operational strategy aimed at improving the thermodynamic stability of the chiller. Second, to demonstrate how effective this new strategy is in minimizing fluctuations in the chilled water outlet temperature around the desired set point of 8.7°C, thereby achieving performance stability comparable

to that of traditional cooling systems. The ultimate goal was to prove that active flow modulation, rather than passive fixed-flow operation, is the key to cyclic steady-state optimization. The key contribution of this study is the creation of an operational scheme that combines an expanded six-mode cycle time of 900 seconds with accurate proportional-integral-derivative (PID) control of the cooling water flow rate in the adsorber bed. While conventional cycles use only four modes, the proposed six-mode allocation enhances heat recovery time, particularly doubling the duration of pre-cooling. This new timing is integrated with the PID controller, which uses 3, 9, and 90 discrete steps to approximate the optimal, continuously varying flow profile. This controlled, variable flow method significantly advances the fixed-flow, on/off controls typically used.

The numerical results unequivocally demonstrate the superior performance and stability of the proposed scheme. The conventional cycle exhibited a large peak-to-peak temperature fluctuation of 3.5°C and a high standard deviation, confirming its instability. In sharp contrast, the PID-controlled cycles drastically reduced this instability. The research identified the 9 discrete step strategy as the optimal compromise for operation, achieving the lowest temperature instability with a peak-to-peak fluctuation of just 0.9°C and the lowest standard deviation (0.30°C), thereby keeping the average temperature closest to the 8.7°C set point. Furthermore, the n=9 strategy significantly boosted energy performance, yielding an improvement in the COP by 5.5% to 0.476 and an increase in CC by 4.9% to 14.62 kW over the conventional cycle baseline, with smoother refrigerant flow (0.05-0.10 kg/s) minimizing thermal imbalances. Finer n=90 steps yielded marginal further gains (COP 0.478, +6.0%, CC 14.74 kW, +5.7%) but slightly higher fluctuations (1.2°C), highlighting a trade-off. While n=90 offers slightly higher gains (COP 0.478, +6.0%, CC 14.74 kW, +5.7%), its increased fluctuations (1.2°C) indicate a trade-off where finer discretization enhances efficiency but may sacrifice stability compared to intermediate steps. The n=9 strategy is demonstrably superior, achieving excellent temperature stability and substantial performance uplift over the conventional baseline. It is the preferred choice as it represents the optimal balance between stability and cost. It minimizes temperature fluctuations, thereby prioritizing user comfort and system reliability, without demanding the highly complex, near-continuous flow modulation (n=90) that would require significantly more sophisticated valves, sensors, and computational overhead. The assumption that the PID controller was perfectly tuned in the simulation environment should be recognized. However, in a real physical system, obtaining the optimal PID gain parameters can be complex and time-consuming. Additionally, these parameters would need to be continually adjusted to account for changing ambient conditions.

The successful implementation of this six-mode, PID-controlled cooling water flow strategy carries profound implications. First, it provides a clear design and operational guideline (the n=9 step approach) for future two-bed adsorption chiller manufacturers seeking to optimize thermal stability. Second, the drastic reduction in temperature fluctuation proves that adsorption chillers can reliably deliver cooling water at a near-constant temperature, directly addressing the major drawback that has limited their commercial viability. Future research should focus on hardware implementation and experimental validation of this n=9 strategy and on extending this multi-step PID approach to other cycle parameters, such as heating water flow, to further maximize overall system performance and drive the adsorption cooling industry toward higher efficiency and wider adoption.

A key limitation of this numerical modeling is the use of lumped-parameter assumptions, which may overlook real-world discrepancies. Specifically, unmodeled factors such as valve delays, fouling, and ambient heat losses could lead to an overestimation of system stability. Additionally, the reliance on

idealized PID tuning may fail to account for hardware noise or actuator dynamics, potentially risking instability in transient systems and resulting in inflated performance gains compared to a physical prototype. Future work should focus on experimental validation involving a lab-scale two-bed silica gel-water prototype with variable-speed controls, comparing experimental data against simulations. Furthermore, integrating advanced computational fluid dynamics (CFD) could refine the model, ensuring the strategy's robustness for sustainable cooling commercialization.

References

[1] Hassan M, El-Sharkawy I, Harby K (2023) Study of an innovative combined absorption–adsorption cooling system employing the same evaporator and condenser. Case Stud Therm Eng 42:102690. https://doi.org/10.1016/j.csite.2022.102690

[2] Hassan M, El-Sharkawy I, Amin MT, Harby K (2023) Numerical simulation of cascaded absorption–two-stage 4-bed adsorption cooling cycles for efficient low-grade heat utilization. Appl Therm Eng 235:121396. https://doi.org/10.1016/j.applthermaleng.2023.121396

[3] Wang J (2022) Comprehensive analysis for state-of-the-art adsorption refrigeration technologies. Highlights Sci Eng Technol 16:2559. https://doi.org/10.54097/hset.v16i.2559

[4] Grzebielec A, Rusowicz A (2013) Analysis of the use of adsorption processes in trigeneration systems. Arch Thermodyn 34:35–49. https://doi.org/10.2478/aoter-2013-0028

[5] Pan Q, Shan H, Tamainot-Telto Z, Wang R (2022) Heat recovery for adsorption refrigeration system via pinch technology. J Therm Sci 31:379–389. https://doi.org/10.1007/s11630-022-1535-7

[6] Sârbu I, Sebarchievici C (2015) General review of solar-powered closed sorption refrigeration systems. Energy Convers Manag 105:403–422. https://doi.org/10.1016/j.enconman.2015.07.084

[7] Wang K, Vineyard E (2011) Adsorption refrigeration system. ASHRAE J 53.

[8] Kim D, Ferreira C (2008) Solar refrigeration options – a state-of-the-art review. Int J Refrig 31:3–15.

[9] Amin M (2024) Performance analysis of a new combined absorption–adsorption refrigeration system to improve energy performance. J Therm Eng 10(3):722-735. https://doi.org/10.14744/thermal.0000822

[10] Cabeza L, Solé A, Barreneche C (2017) Review on sorption materials and technologies for heat pumps and thermal energy storage. Renew Energy 110:3–39. https://doi.org/10.1016/j.renene.2016.09.059

[11] Mukhtar H, Ghani S (2021) Hybrid ejector-absorption refrigeration systems: A review. Energies 14(20):6576. https://doi.org/10.3390/en14206576

[12] Chauhan P, Kaushik S, Tyagi S (2022) Current status and technological advancements in adsorption refrigeration systems: A review. Renew Sustain Energy Rev 154:111808. https://doi.org/10.1016/j.rser.2021.111808

[13] 13 P, Sur A, Gaba V, Sah R (2021) Review on improvement of adsorption refrigeration systems performance using composite adsorbent. Energy Sources Part A 47:8031–8055. https://doi.org/10.1080/15567036.2021.1927252

[14] Satheeshkumar P, Selwynraj A (2024) Pathways to enhance the performance of adsorption cooling system: An overview. Results Eng 23:102855. https://doi.org/10.1016/j.rineng.2024.102855

[15] Saha BB, Koyama S, Lee JB, Kuwahara K, Alam KCA, Hamamoto Y, Akisawa A, Kashiwagi T (2003a) Performance evaluation of a low-temperature waste-heat-driven multi-bed adsorption chiller. Int J Multiphase Flow 29:1249–1263.

[16] Pendurthi M, Pelluru V, Chilakapati A, Dandotiya D, Banker N (2021) Performance investigation of a vapor adsorption refrigeration system based on adsorption/desorption time and heat transfer. J Therm Sci Eng Appl 13(5):051024. https://doi.org/10.1115/1.4050230

[17] Szarzynski S, Feng Y, Pons M (1997) Study of different internal vapor transports for adsorption cycles with heat regeneration. Int J Refrig 20(6):390–401.

[18] Wang RZ (2001) Performance improvement of adsorption cooling by heat and mass recovery operation. Int J Refrig 24:602–611.

[19] Saha BB, Koyama S, Kashiwagi T, Akisawa A, Ng KC, Chua HT (2003b) Waste heat–driven dual-mode, multi-stage, multi-bed regenerative adsorption system. Int J Refrig 26(7):749–757.

[20] Saha BB, Koyama S, Ng KC, Hamamoto Y, Akisawa A, Kashiwagi T (2006) Study on a dual-mode, multi-stage, multi-bed regenerative adsorption chiller. Renew Energy 31:2076–2090.

[21] Lukyanov V, Bo-Dakkah B, Sultanguzin I, Kurzanov S, Yavorovsky Y, Skorobatyuk A (2025) Absorption and adsorption cooling cycles for residential applications in Moscow region. Proc IEEE REEPE:1–6. https://doi.org/10.1109/reepe63962.2025.10971004

[22] El-Sharkawy I, AbdelMeguid H, Saha B (2013) Towards an optimal performance of adsorption chillers: Reallocation of adsorption/desorption cycle times. Int J Heat Mass Transf 63:171–182. https://doi.org/10.1016/j.ijheatmasstransfer.2013.03.076

[23] Gado M, Elgendy E, Elsayed K, Fatouh M (2019) Performance enhancement of an adsorption chiller by optimum cycle time allocation at different operating conditions. Adv Mech Eng 11(10). https://doi.org/10.1177/1687814019884780

[24] Pan Q, Wang R, Wang L, Liu D (2016) Design and experimental study of a silica gel-water adsorption chiller with modular adsorbers. Int J Refrig 67:336–344. https://doi.org/10.1016/j.ijrefrig.2016.03.001

[25] Youssef P, Mahmoud S, Al-Dadah R (2015) Performance analysis of four-bed adsorption water desalination/Refrigeration system: Comparison of AQSOA-Z02 to silica gel. Desalination 375:100–107. https://doi.org/10.1016/j.desal.2015.08.002

[26] Sztekler K, Kalawa W, Nowak W, Mika L, Grądziel S, Krzywański J, Radomska E (2020) Experimental study of three-bed adsorption chiller with desalination function. Energies13(21):5827. https://doi.org/10.3390/en13215827

[27] Alsarayreh A, Al-Maaitah A, Attarakih M, Bart H (2021) Energy and exergy analyses of adsorption chiller at various recooling-water and dead-state temperatures. Energies 14:2172. https://doi.org/10.3390/en14082172

[28] Lee J, Bae K, Kwon O (2020) Performance investigation of a two-bed type adsorption chiller with various adsorbents. Energies 13(10):2553. https://doi.org/10.3390/en13102553

[29] Lee W, Park M, Duong X, Koushaeian M, Shah N, Chung J (2021) Time allocation of a three-bed adsorption chiller using an artificial neural network. Case Stud Therm Eng 28:101553. https://doi.org/10.1016/j.csite.2021.101553

[30] Alam KCA, Kang YT, Saha BB, Akisawa A, Kashiwagi T (2003) A novel approach to determine optimum switching frequency of a conventional adsorption chiller. Energy 28:1021–1037.

[31] Toppi T, Villa T, Vasta S, Mittelbach W, Freni A (2022) Testing of a falling-film evaporator for adsorption chillers. Energies 15(5):1709. https://doi.org/10.3390/en15051709

[32] Aprile M, Di Cicco A, Toppi T, Freni A, Motta M (2022) Modelling of a falling-film evaporator for adsorption chillers. Int J Refrig 146:471-482. https://doi.org/10.1016/j.ijrefrig.2022.12.009

[33] Begum FA, Mzi K, Rouf RA, Kca A (2018) Effect of flow rate on performance of solar adsorption chiller keeping fixed evaporator outlet temperature. J Appl Mech Eng 7(4). https://doi.org/10.4172/2168-9873.1000310

[34] Elsheniti MB, El-Hamid ATA, Samni OAE, Elsherbiny SM, Elsayed E (2021) Experimental evaluation of a solar two-bed lab-scale adsorption cooling system. Alex Eng J 60(3):2747–2757. https://doi.org/10.1016/j.aej.2021.01.024

[35] Villa AAO, Dutra JCC, Henríquez JR, Dos Santos CAC, Da Costa JÂP (2019) Dynamic experimental analysis of a LiBr/H_2O single-effect absorption chiller (35 kW). Acta Sci Technol 41(1):35173. https://doi.org/10.4025/actascitechnol.v41i1.35173

[36] Xia Z, Wang D, Zhang J (2007) Experimental study on improved two-bed silica gel–water adsorption chiller. Energy Convers Manag 49(6):1469-1479. https://doi.org/10.1016/j.enconman.2007.12.019

[37] Kareem F, Khalifa A, Hamad A (2023) Numerical analysis of two-bed adsorption thermophysical battery. Appl Therm Eng Part D 236:121847. https://doi.org/10.1016/j.applthermaleng.2023.121847

[38] Makahleh F, Badran A, Attar H, Amer A, Al-Maaitah A (2022) Modeling and simulation of a two-stage air-cooled adsorption chiller with heat recovery part II: Parametric study. Appl Sci 12(10):5156. https://doi.org/10.3390/app12105156

[39] Khatun G, Khan M (2025) Effect of chilled water outlet temperature on the performance of a three-bed adsorption chiller. Int J Math Stat Stud 13(2):43-52. https://doi.org/10.37745/ijmss.13/vol13n24352

[40] Rouf R, Alam K, Saha B, Kabir K (2019) Utilizing accessible heat enhancing cooling effect with three-bed solar adsorption chiller. Heat Transf Eng 40:1049–1059. https://doi.org/10.1080/01457632.2018.1451244

[41] Rouf R, Jahan N, Alam K, Sultan A, Saha B, Saha S (2020) Improved cooling capacity of a solar heat-driven adsorption chiller. Case Stud Therm Eng 17:100568. https://doi.org/10.1016/j.csite.2019.100568

[42] Saha BB, Boelman EC, Kashiwagi T (1995) Computer simulation of a silica gel–water adsorption refrigeration cycle: Influence of operating conditions on cooling output and COP. ASHRAE Trans 101(2):348–357.

[43] Sakoda A, Suzuki M (1984) Fundamental study on solar powered adsorption cooling system. J Chem Eng Jpn 17(1):52–57.

[44] Dawoud B, Vedder U, Amer EH, Dunne S (2007) Non-isothermal adsorption kinetics of water vapour into a consolidated zeolite layer. Int J Heat Mass Transf 50:2190–2199. https://doi.org/10.1016/j.ijheatmasstransfer.2006.10.052

[45] Chua HT, Ng KC, Wang W, Yap C, Wang XL (2004) Transient modeling of a two-bed silica gel–water adsorption chiller. Int J Heat Mass Transf 47(4):659–669.

[46] Hui J (2024) Discrete-time integral terminal sliding mode load following controller coupled with disturbance observer for a modular high-temperature gas-cooled reactor. Energy 292:130479. https://doi.org/10.1016/j.energy.2024.130479

Statements and Declarations

Author Contributions: M. Hassan conducted the numerical simulations and performed the initial draft writing. A. Bagabir was responsible for the literature review, analysis of the results, and the final review and editing of the manuscript. All authors have read and agreed to the published version of the manuscript.

Funding: The authors declare that no funds, grants, or other support were received during the preparation of this manuscript.

Competing Interests: The authors have no relevant financial or non-financial interests to disclose.

Data Availability Statement: The computational datasets generated and analyzed during the current study are available from the corresponding author upon reasonable request. Numerical simulations were conducted using MATLAB and Microsoft Excel for XY plots. While the raw simulation files are not included in the manuscript, they can be shared with interested researchers for academic and non-commercial purposes, subject to institutional and software license compliance. All relevant input parameters, and model details are fully described in the manuscript to ensure reproducibility.

Table 1 Time operation of the four-mode conventional cycle.

Mode	A	B	C	D
Time	420 s	30 s	420 s	30 s
Bed 1	Adsorption	Pre heating	Desorption	Pre cooling
Bed 2	Desorption	Pre cooling	Adsorption	Pre heating

Table 2 Time operation of the six-mode cycle.

Mode	A	B	C	D	E	F
Time	30 s	360 s	60 s	30 s	360 s	60 s
Bed 1	Preheating	Desorption	Pre cooling	Adsorption		
Bed 2	Adsorption			Preheating	Desorption	Precooling

Table 3 Values of the parameters adopted in Eqs. (2) and (3).

A_0	A_1	A_2	A_3
-6.5314	0.072452	-0.23951×10^{-3}	0.25493×10^{-3}
B_0	B_1	B_2	B_3
-15.587	0.15915	-0.50612×10^{-3}	0.5329×10^{-6}

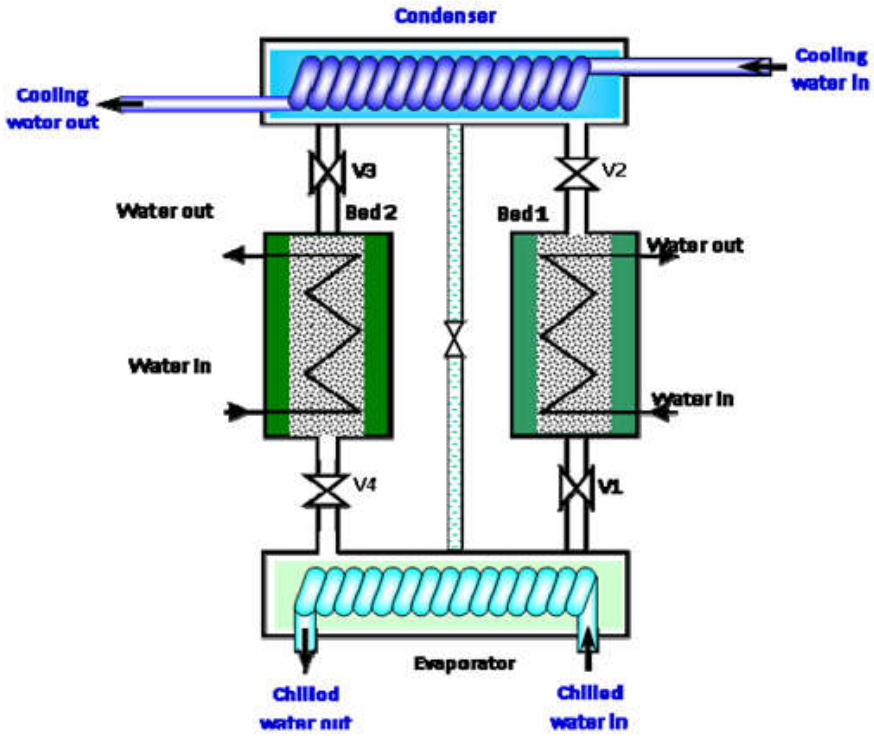

Fig. 1 Schematic diagram of two-bed adsorption chiller.

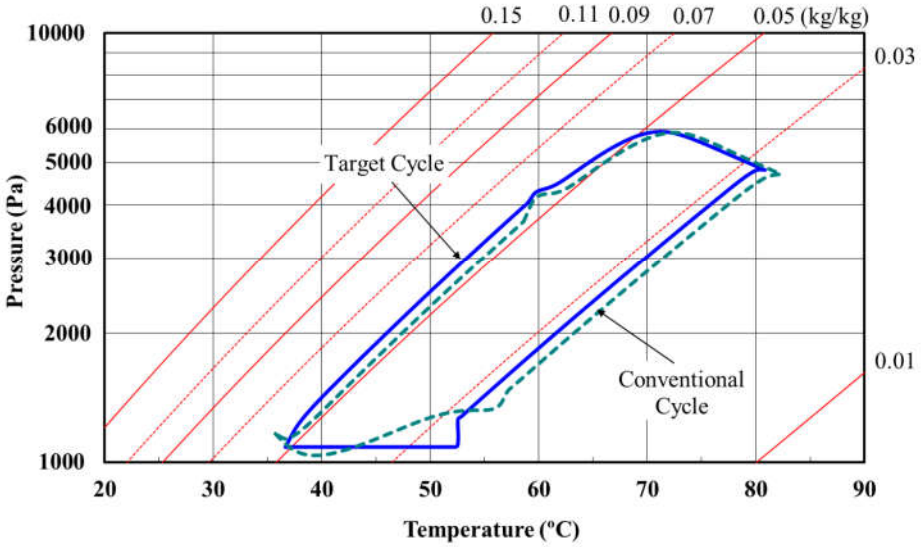

Fig. 2 *P-T-W* diagram compares the target cycle (constant evaporator temperature cycle) and the conventional cycle

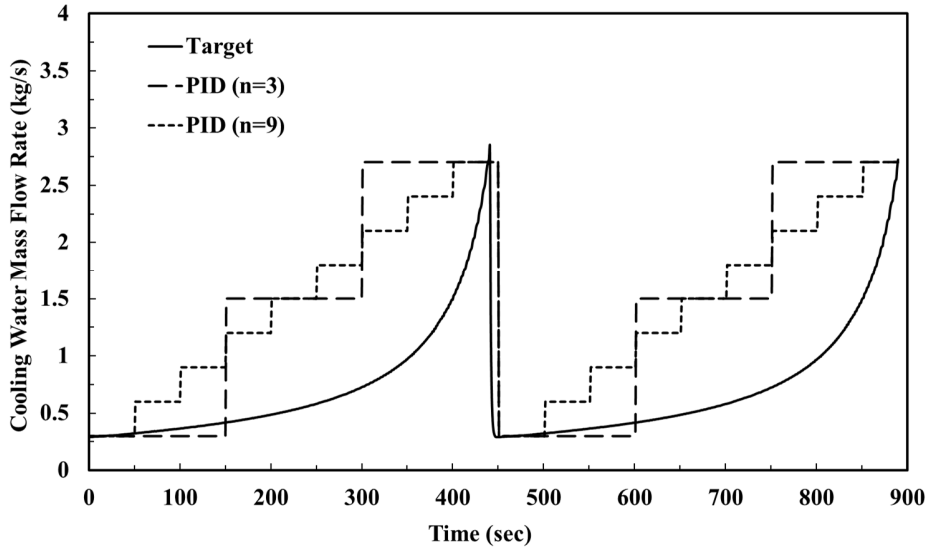

Fig. 3 Cooling water flow profiles for the discrete steps 3 and 9, compared with the target cycle.

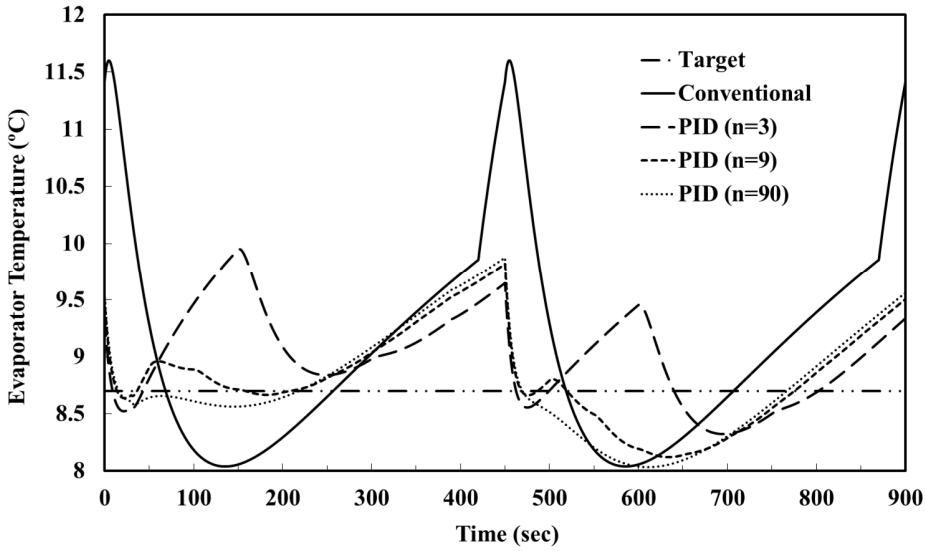

Fig. 4 Evaporator outlet temperature profiles for different cooling water flow schemes compared with the conventional cycle.

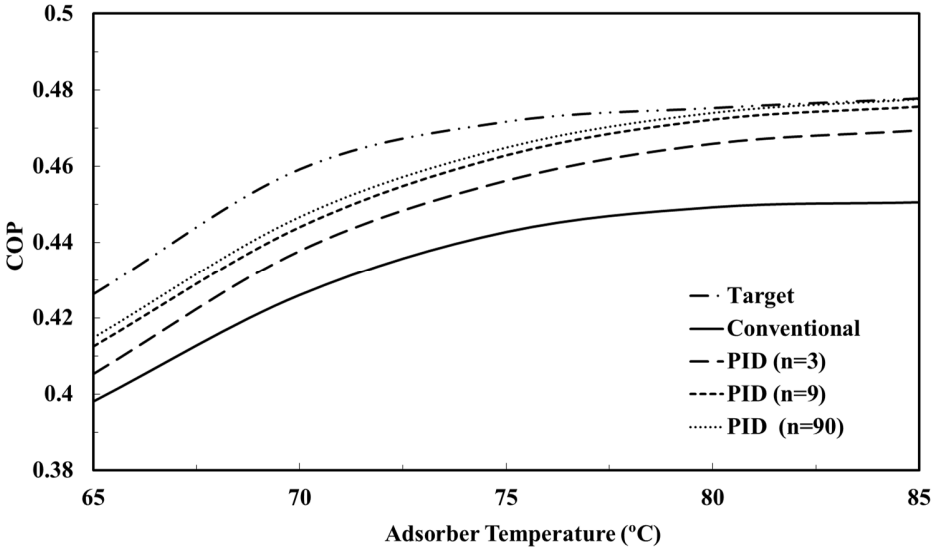

Fig. 5 Coefficient of Performance (COP) for different cooling water flow schemes compared with the conventional cycle.

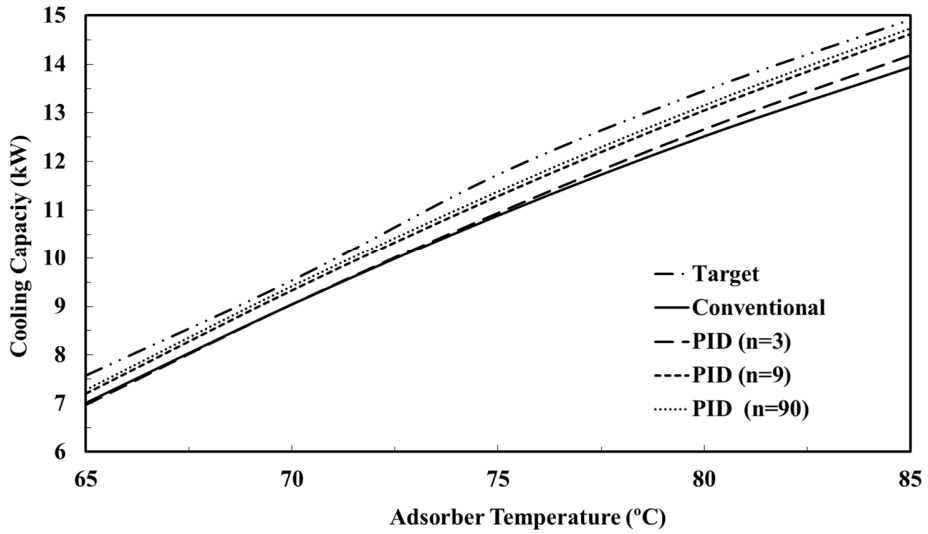

Fig. 6 Cooling capacity (CC) for different cooling water flow schemes compared with the conventional cycle.

Table 4 Comparison between the conventional cycle and different discrete-step schemes.

Scheme	Fluctuation (T°C)		Maximum Performance	
	Peak-to-Peak	SD	COP	CC (kW)
Conventional cycle	3.5	1.34	0.451	13.94
PID (n=3)	1.5	0.54	0.469	14.18
PID (n=9)	0.9	0.30	0.476	14.62
PID (n=90)	1.2	0.43	0.478	14.74

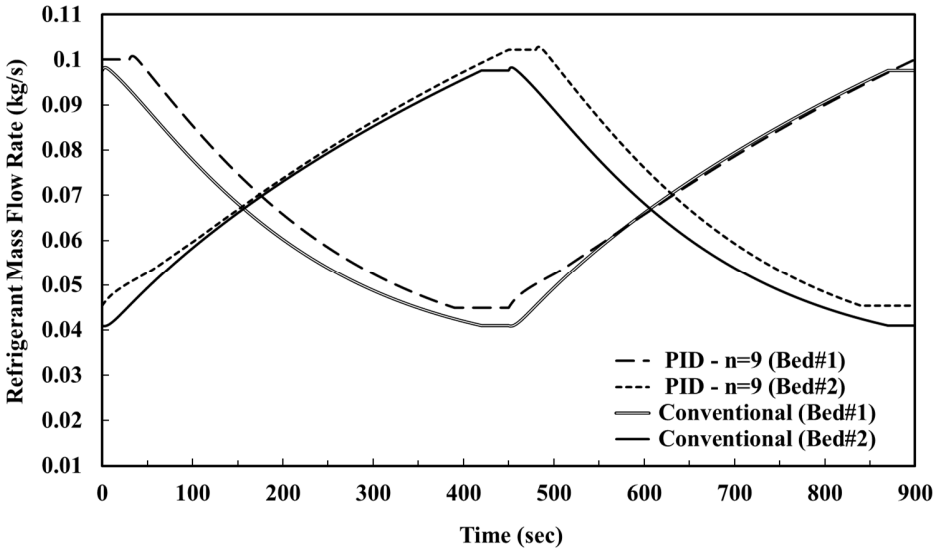

Fig. 7 Adsorbate mass variation in beds for the PID control of 9 steps compared with the conventional cycle.